# Rotationally resolved $\tilde{A}\ ^2\Pi_g \leftarrow \tilde{X}\ ^2\Pi_u$ electronic spectrum of triacetylene cation by frequency modulation absorption spectroscopy

Wayne E. Sinclair, David Pfluger, Harold Linnartz, and John P. Maier
*Institute for Physical Chemistry, University of Basel, Klingelbergstrasse 80, CH 4056 Basel, Switzerland*

(Received 14 August 1998; accepted 25 September 1998)

The spectrum of the $\tilde{A}\ ^2\Pi_g \leftarrow \tilde{X}\ ^2\Pi_u\ 0_0^0$ band system of the triacetylene cation and isotopic derivatives $DC_6H^+$ and $C_6D_2^+$ have been studied at Doppler-limited resolution using frequency modulation absorption spectroscopy. The ions were generated in a liquid-nitrogen-cooled hollow cathode discharge incorporated in a White cell. A discharge modulation in combination with the frequency modulation technique was used to enhance the detection sensitivity. Analyses of the rotational structure yield accurate rotational and spin-orbit interaction constants of triacetylene cation in the two electronic states and information on its geometry. © *1999 American Institute of Physics.* [S0021-9606(99)01501-9]

## I. INTRODUCTION

The carbon-chain triacetylene radical cation ($C_6H_2^+$) is a member of the polyacetylene series which has been considered as an important intermediate species in combustion, plasmas, and planetary and interstellar gas-phase ion-molecule reaction schemes. It has long been the aim to study electronic transitions of these species in order to better understand their role in such environments. The $\tilde{A}\ ^2\Pi_u \rightarrow \tilde{X}\ ^2\Pi_g$ emission band system of diacetylene cation ($C_4H_2^+$) was the first identified emission spectrum of the series following the assignment of Schüler's ''*T*'' spectrum[1] in 1956.[2] Subsequently, the corresponding gas-phase transitions of $C_nH_2^+$, $n=6,8$ have been observed via their emission spectra of molecular beams excited by electron impact.[3] Prior to the work reported here, $C_4H_2^+$ was the only such species for which the rotationally resolved electronic spectrum was analyzed.[2,4,5] In this paper, a detailed study of the rotationally resolved $\tilde{A}\ ^2\Pi_g \leftarrow \tilde{X}\ ^2\Pi_u\ 0_0^0$ electronic transition of $C_6H_2^+$ and isotopic derivatives $DC_6H^+$ and $C_6D_2^+$ is presented.

Several gas-phase studies of the $\tilde{A}\ ^2\Pi_g \leftrightarrow \tilde{X}\ ^2\Pi_u$ transition of $C_6H_2^+$ have been made. The $\tilde{A}\ ^2\Pi_g \rightarrow \tilde{X}\ ^2\Pi_u\ 0_0^0$ electronic transition was observed for the first time in 1976 in the gas phase in an emission spectrum employing low-energy electron impact excitation on an effusive beam.[3] In a later study, the emission and laser excitation spectra of rotationally cooled $C_6H_2^+$ were obtained.[6] A band structure consisting of two components separated by $\approx 2\ cm^{-1}$ was apparent in the low resolution spectrum. The two sub-bands were attributed to the overlapping two spin-orbit systems, $^2\Pi_{1/2,g} \leftarrow {}^2\Pi_{1/2,u}$ and $^2\Pi_{3/2,g} \leftarrow {}^2\Pi_{3/2,u}$. Higher resolution scans in emission at rotational temperatures of 5–10 K revealed only the unresolved red-shaded *R* branches of the two spin-orbit components. From a direct comparison with the rotationally resolved and analyzed emission spectrum of diacetylene cation, a tentative observation of the $Q_{3/2}$ branch head was associated with the higher energy sub-band. These observations were consistent with the band of the $\Omega=3/2$ system lying to higher energy than that of the $\Omega=1/2$ system, and that $B'(\tilde{A}\ ^2\Pi_g) < B''(\tilde{X}\ ^2\Pi_u)$. As the cationic states are inverted, it also followed that $|A'| < |A''|$.

Because rotational fine structure was not resolved in the previous studies, rotational or spin-orbit constants could not be derived. As a consequence, an experimental setup to study the high resolution $\tilde{A}\ ^2\Pi_g \leftarrow \tilde{X}\ ^2\Pi_u\ 0_0^0$ electronic spectrum of $C_6H_2^+$, using the combined techniques of discharge modulation and frequency modulation (FM) laser absorption spectroscopy, was developed. Discharge modulation, coupled with phase sensitive detection, is a commonly adopted technique to achieve a high degree of sensitivity and selectivity in the spectroscopic detection of transient species. FM absorption spectroscopy is a well established technique based on the method of optical heterodyne spectroscopy. The technique utilizes an external phase modulator to produce a wavelength modulation and has proven to be a sensitive absorption method to detect stable molecules.[7,8] It has also been demonstrated that by combining FM with other forms of absorption spectroscopy, the sensitivity for detecting weak absorptions is enhanced considerably. A notable example is the combination of FM with magnetic rotation spectroscopy.[9,10] In addition, FM spectroscopy, in combination with a modulation of the absorbing species, is capable of detecting transient species with both high resolution and high sensitivity.[11–14] The technique has been used to probe real-time kinetics of chemical processes and to obtain high resolution Doppler-limited vibronic spectra of photochemically generated radicals mainly in the groups of Sears and Hall at Brookhaven National Laboratory.[11,15–18]

In the present work, the techniques of FM spectroscopy with discharge modulation of ions generated in a hollow cathode discharge have been combined to obtain Doppler-limited absorption spectra of the $\tilde{A}\ ^2\Pi_g \leftarrow \tilde{X}\ ^2\Pi_u\ 0_0^0$ band system of $C_6H_2^+$ as well as its isotopic species $DC_6H^+$ and $C_6D_2^+$. The analyses of the fully resolved rotational structure yield for the first time accurate values of the rotational and spin-orbit constants in the $\tilde{X}\ ^2\Pi_u$ and $\tilde{A}\ ^2\Pi_g$ states.

 

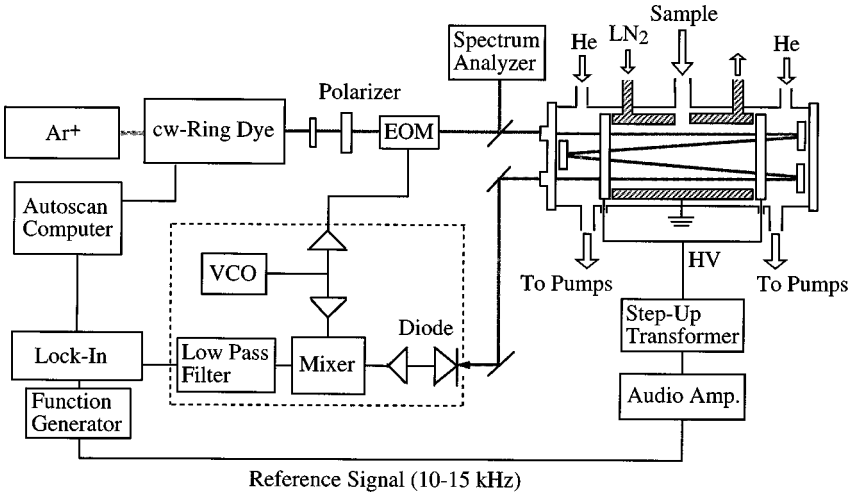


FIG. 1. Schematic diagram of the experimental apparatus.

## II. EXPERIMENT

Figure 1 shows schematically the experimental setup. The $C_6H_2^+$, $DC_6H^+$, and $C_6D_2^+$ ions were produced in a liquid-nitrogen-cooled hollow cathode discharge cell. The cathode consisted of a refrigerant reservoir formed from two concentrically arranged stainless steel tubes (136 cm long), sealed at the ends, and with liquid-nitrogen inlets near each end. A pair of stainless steel (4 cm long) electrodes placed coaxially with the cathode, with a separation of 7 cm, formed the anodes. The discharge assembly was mounted inside a stainless steel (2 m long, 12 cm diameter) White-type multireflection absorption cell by Teflon spacers. The effective optical path length was about 100 m. The cathode was cooled with a continuous flow of liquid nitrogen through the reservoir. The absorption cell was surrounded by foam cladding to provide some thermal insulation. Mechanical shields were mounted directly in front of the mirrors to restrict the deposition of contaminants onto the surfaces. In addition, helium blows directly at the surface of the mirrors, creating a protective curtain. A 170 $m^3$/h roots pump backed by a 100 $m^3$/h double-stage rotary pump was used to evacuate the cell through outlets at both ends and to maintain the background pressure below $10^{-3}$ mbar. The AC high voltage was driven by a sine-wave (10–15 kHz) generator, amplified by an 1200 W audio amplifier and stepped-up by a line transformer. This voltage was then rectified and applied to the anodes while the cathode was kept at earth potential. The peak voltage was measured to be 0.5 kV with a peak to peak current of 200 mA in a pure helium discharge. The $C_6H_2^+$ and $C_6D_2^+$ ions were produced by introducing a gas mixture of 0.5%–1.0% of $C_2H_2$ or $C_2D_2$ diluted in He into the hollow cathode through a central inlet. For the production of the $DC_6H^+$ ion, a gas mixture ratio of $C_2D_2$: $C_2H_2 \approx 3{:}1$ gave the best results. The stagnation pressure was kept at 1.0–1.5 mbar and a temperature of 150–170 K was achieved in the cathode discharge.

The FM technique, in combination with production modulation, was employed to accomplish higher sensitivity for detecting weak absorption signals. The probe laser was a single-mode ring-dye laser pumped by an 8 W cw $Ar^+$ laser and operating near 600 nm. The output of the laser was phase-modulated by a $MgO{:}LiNbO_3$ electro-optic modulator (EOM) driven by about 1 W of radio frequency power at 192 MHz. A Fabry-Perot étalon spectral analyzer monitored the depth of modulation of the carrier frequency. Radio frequency power into the modulator was adjusted to give first order sidebands typically 25% of the carrier frequency intensity. The frequency-modulated laser beam was passed through the discharge cell and focused onto a fast photodiode for signal acquisition. A neutral density filter was used to adjust the power on the diode to about 10–15 mW. The high frequency components of the photodiode were amplified and demodulated in a double balanced mixer, referenced to the local radio frequency source which drives the EOM. The output of the mixer was filtered with a 65 MHz low pass filter to attenuate the $2f$ signal at 380 MHz. The photodiode signal was fed to a lock-in amplifier, to demodulate the signal at the discharge modulation frequency. Spectra were recorded with a time constant of 1 s and a sensitivity of 50 to 200 $\mu$V. A PC with an autoscan system software served to collect the data and to record the spectra. Absolute frequency calibration was performed by simultaneously recording the $I_2$ absorption spectrum with an estimated accuracy of better than 0.005 $cm^{-1}$.

FM signals are recorded as a derivative-like form of the real absorption feature resulting from the fact that the sideband splitting is comparable to the Doppler width of the rovibronic transitions. A true reconstruction of Doppler-broadened line shapes from FM line profiles is not trivial.[19] Nevertheless, the separation of positive and negative peaks corresponds roughly to the real absorption linewidth [full width at half maximum (FWHM)]. To determine the frequencies of the absorption lines, a numerical integration was performed on the FM signal. The resulting rotationally resolved spectra were analyzed using a simulation program, PGOPHER.[20]

## III. RESULTS AND DISCUSSION

The high resolution FM spectrum of the $0_0^0$ band of the $\tilde{A}\ ^2\Pi_g \leftarrow \tilde{X}\ ^2\Pi_u$ electronic transition of $C_6H_2^+$ was recorded

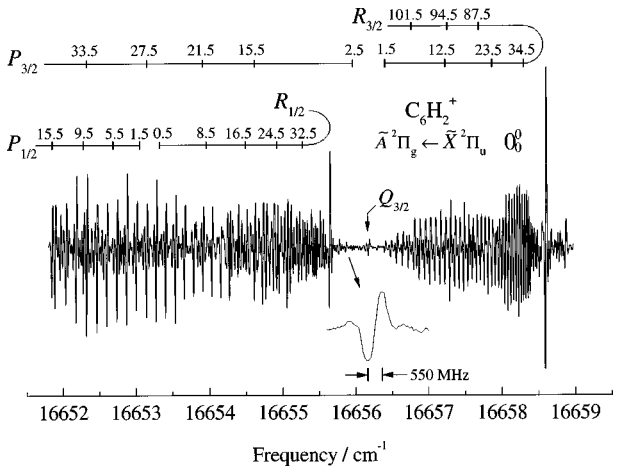


FIG. 2. Part of the rotationally resolved FM absorption spectrum of the $\tilde{A}\,^2\Pi_g \leftarrow \tilde{X}\,^2\Pi_u$ $0_0^0$ electronic transition of $C_6H_2^+$, recorded with a liquid-nitrogen-cooled hollow cathode discharge of a $C_2H_2$/He mixture. The 3/2 and 1/2 subscripts of the rotational branch labels refer to the two spin-orbit components. The rotational assignments of the sub-bands are given at the top of the spectrum. The position of the $Q_{3/2}$ branch head is indicated. The width shown in the expanded measured line shape of the $P(3.5)$ rovibronic transition corresponds roughly to the FWHM.

in the range 16 640–16 660 cm$^{-1}$. A portion of the $0_0^0$ band of $C_6H_2^+$ is shown in Fig. 2. The spectrum exhibits clearly resolved rotational structure with rovibronic linewidths (FWHM) of roughly 550 MHz for Doppler-broadened $C_6H_2^+$ signals (see expanded portion of Fig. 2). The rotational temperature is assumed to be equilibrated with the translational temperature in the hollow cathode discharge. The observed FWHM corresponds to a translational temperature of about 170 K. Two prominent band heads separated by about 3 cm$^{-1}$ are found toward the blue end of the spectrum. The rotational structure is red-shaded, indicating that $B' < B''$ and thus that the band heads belong to $R$ branches. As marked in Fig. 2, each band head is associated with one sub-band comprised of strong, well defined $P$ and $R$ branches extending from a relatively weak $Q$ branch head near the origin. The higher energy sub-band displays measurably more intensity. Similar qualitative features were observed for the $0_0^0$ bands of $DC_6H^+$ and $C_6D_2^+$ in the ranges 16 660–16 675 and 16 675–16 690 cm$^{-1}$, respectively.

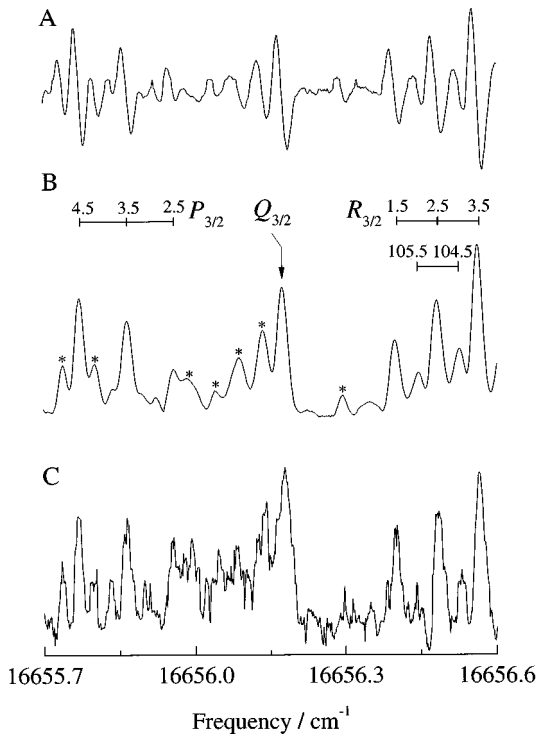


FIG. 3. Portion of the $C_6H_2^+$ spectrum in the region of the band center of the $^2\Pi_{3/2} \leftarrow {}^2\Pi_{3/2}$ sub-band showing the prominent $Q_{3/2}$ branch band head. (a) FM absorption signal. (b) Integration of the FM spectrum in (a). Rotational assignments are indicated above each band. Asterisks indicate the most prominent peaks not part of this band system. (c) The same part of the absorption spectrum, using only the discharge modulation technique obtained under comparable scan conditions.

It appears that the $0_0^0$ $\tilde{A}\,^2\Pi_g \leftarrow \tilde{X}\,^2\Pi_u$ electronic transition of $C_6H_2^+$ is split into two subsystems. This feature was already observed in the low resolution emission spectroscopic study.[6] However, the spectrum showed only the unresolved $R$ branches of the two spin-orbit components; the corresponding spectra of $DC_6H^+$ and $C_6D_2^+$ were not studied. The two sub-bands are attributed to the resolution of two closely overlapping spin-orbit systems, $\tilde{A}\,^2\Pi_{1/2,g} \leftarrow \tilde{X}\,^2\Pi_{1/2,u}$ and $\tilde{A}\,^2\Pi_{3/2,g} \leftarrow \tilde{X}\,^2\Pi_{3/2,u}$, separated by the difference in the spin-orbit interaction constants for each electronic state $|A' - A''|$. The molecular orbital configuration describing $C_6H_2^+$ in the $\tilde{X}\,^2\Pi_u$ and $\tilde{A}\,^2\Pi_g$ states is $\ldots(\pi_u)^4(\pi_g)^4(\pi_u)^3$ and $\ldots(\pi_u)^4(\pi_g)^3(\pi_u)^4$, respectively. Thus, the $^2\Pi$ ground state of $C_6H_2^+$ is inverted, i.e., $\Omega = 3/2$ component is lower lying than the $\Omega = 1/2$ one, with $A$ having a negative value. The spin-orbit constants in the $\tilde{X}\,^2\Pi_u$ and $\tilde{A}\,^2\Pi_g$ states are expected to be close to those determined for the related polyacetylene species, $C_4H_2^+$. The spin-orbit constants of $C_4H_2^+$ in its $\tilde{X}\,^2\Pi_u$ state has been determined to be $-33.6$ cm$^{-1}$.[2,4] Furthermore, the rotational constant of $C_6H_2^+$ is expected to be significantly smaller than the spin-orbit splitting, and thus for the lower $J$ levels, the $^2\Pi_g \leftarrow {}^2\Pi_u$ electronic transition belongs to Hund's case (a). However, for transitions with sufficiently high $J$ values, the lines may further split into $\Lambda$-doublets.

Most significant in the FM spectrum of Fig. 2 is the clearly discernible $Q_{3/2}$ branch head at 16 656.17 cm$^{-1}$. The $Q$ branch in transitions of this type is expected to be very weak at the high ambient temperature of the experiment that favors a population distribution over many rotational levels, because in electronic transitions with $\Delta\Lambda = 0$ the $Q$-line strength $S_{JJ}$ is given by $S_{JJ} = \Omega^2(2J+1)/J(J+1)$. The corresponding branch heads in the $0_0^0$ bands of $DC_6H^+$ and $C_6D_2^+$ are shifted to the blue by 15.9 and 31.7 cm$^{-1}$, respectively. In Fig. 3(a), the part of the FM absorption spectrum in the region of the $Q_{3/2}$ branch head is displayed. Figure 3(b) shows the real absorption spectrum derived from the FM data of Fig. 3(a) and demonstrates an excellent signal-to-noise ratio. In order to demonstrate the improvement in signal to noise achieved by the double modulation technique, the same spectral region in Fig. 3(a) was recorded under similar scan conditions but employing only discharge modulation. The result is shown in Fig. 3(c). A comparison of

TABLE I. Frequencies (in $cm^{-1}$) and assignments for the $\tilde{A}\ ^2\Pi_g \leftarrow \tilde{X}\ ^2\Pi_u\ 0_0^0$ absorption spectrum of $C_6H_2^+$ and residuals from the fit.

| $J$ | obs. | $o$-$c$[a] | $J$ | obs. | $o$-$c$[a] | $J$ | obs. | $o$-$c$[a] | $J$ | obs. | $o$-$c$[a] | $J$ | obs. | $o$-$c$[a] | $J$ | obs. | $o$-$c$[a] | $J$ | obs. | $o$-$c$[a] |
|---|---|---|---|---|---|---|---|---|---|---|---|---|---|---|---|---|---|---|---|---|
| $R_{3/2}(J)$ | | | | | | $P_{3/2}(J)$ | | | | | | $R_{1/2}(J)$ | | | $P_{1/2}(J)$ | | | | | |
| 1.5 | 16 656.404 | 2 | 83.5 | 16 657.886 | −2 | 2.5 | 16 655.958 | −2 | 52.5 | 16 649.334 | 1 | 0.5 | 16 653.323 | 2 | 1.5 | 16 653.049 | −2 | 45.5 | 16 647.516 | −4 |
| 2.5 | 16 656.485 | 1 | 84.5 | 16 657.842 | 3 | 3.5 | 16 655.865 | −2 | 53.5 | 16 649.162 | 3 | 1.5 | 16 653.407 | 0 | 2.5 | 16 652.965 | 1 | 46.5 | 16 647.349 | −1 |
| 3.5 | 16 656.567 | 1 | 85.5 | 16 657.790 | 1 | 4.5 | 16 655.772 | −1 | 54.5 | 16 648.989 | 5 | 2.5 | 16 653.494 | 4 | 3.5 | 16 652.869 | 2 | 47.5 | 16 647.185 | −2 |
| 4.5 | 16 656.647 | 0 | 86.5 | 16 657.741 | 3 | 5.5 | 16 655.677 | 1 | 55.5 | 16 648.808 | 2 | 3.5 | 16 653.575 | 3 | 4.5 | 16 652.775 | −1 | 48.5 | 16 647.018 | −4 |
| 5.5 | 16 656.727 | 2 | 87.5 | 16 657.683 | −2 | 11.5 | 16 655.062 | −2 | 56.5 | 16 648.630 | 1 | 4.5 | 16 653.650 | −3 | 5.5 | 16 652.676 | −3 | 49.5 | 16 646.851 | −4 |
| 6.5 | 16 656.802 | 0 | 88.5 | 16 657.630 | 1 | 14.5 | 16 654.739 | 3 | 57.5 | 16 648.447 | −2 | 5.5 | 16 653.729 | −3 | 6.5 | 16 652.578 | −4 | 50.5 | 16 646.684 | −3 |
| 7.5 | 16 656.879 | 1 | 89.5 | 16 657.572 | 0 | 15.5 | 16 654.623 | −1 | 58.5 | 16 648.264 | −3 | 6.5 | 16 653.812 | 3 | 7.5 | 16 652.484 | 2 | 51.5 | 16 646.516 | −1 |
| 8.5 | 16 656.951 | 1 | 90.5 | 16 657.514 | 0 | 16.5 | 16 654.508 | −2 | 59.5 | 16 648.082 | −2 | 7.5 | 16 653.883 | −2 | 8.5 | 16 652.379 | −2 | 52.5 | 16 646.346 | 0 |
| 9.5 | 16 657.026 | 2 | 91.5 | 16 657.453 | −1 | 17.5 | 16 654.392 | −3 | 60.5 | 16 647.900 | 1 | 8.5 | 16 653.957 | −2 | 9.5 | 16 652.276 | −2 | 53.5 | 16 646.168 | −5 |
| 10.5 | 16 657.096 | 2 | 92.5 | 16 657.394 | 1 | 18.5 | 16 654.276 | −2 | 61.5 | 16 647.710 | −3 | 9.5 | 16 654.035 | 4 | 10.5 | 16 652.174 | 1 | 54.5 | 16 645.999 | 1 |
| 11.5 | 16 657.163 | −1 | 93.5 | 16 657.329 | −1 | 19.5 | 16 654.156 | −3 | 62.5 | 16 647.522 | −3 | 10.5 | 16 654.102 | −1 | 11.5 | 16 652.067 | 1 | 55.5 | 16 645.819 | −3 |
| 12.5 | 16 657.229 | −1 | 94.5 | 16 657.263 | −3 | 20.5 | 16 654.035 | −2 | 63.5 | 16 647.337 | 2 | 11.5 | 16 654.169 | −3 | 12.5 | 16 651.957 | −2 | 56.5 | 16 645.642 | −2 |
| 13.5 | 16 657.294 | −2 | 95.5 | 16 657.198 | −2 | 21.5 | 16 653.914 | −2 | 64.5 | 16 647.143 | −1 | 12.5 | 16 654.236 | −4 | 13.5 | 16 651.847 | −3 | 57.5 | 16 645.462 | −3 |
| 14.5 | 16 657.361 | 1 | 96.5 | 16 657.133 | 1 | 22.5 | 16 653.790 | −2 | 65.5 | 16 646.948 | −3 | 13.5 | 16 654.302 | −4 | 14.5 | 16 651.743 | 4 | 58.5 | 16 645.283 | −1 |
| 15.5 | 16 657.423 | 0 | 97.5 | 16 657.064 | 2 | 23.5 | 16 653.664 | −3 | 66.5 | 16 646.755 | −3 | 14.5 | 16 654.367 | −3 | 15.5 | 16 651.627 | 0 | 59.5 | 16 645.100 | −2 |
| 16.5 | 16 657.484 | 1 | 98.5 | 16 656.996 | 3 | 24.5 | 16 653.538 | −1 | 67.5 | 16 646.559 | −2 | 15.5 | 16 654.431 | −2 | 16.5 | 16 651.512 | −1 | 60.5 | 16 644.920 | 2 |
| 17.5 | 16 657.543 | 0 | 99.5 | 16 656.919 | 1 | 25.5 | 16 653.408 | −3 | 68.5 | 16 646.361 | −2 | 16.5 | 16 654.493 | −2 | 17.5 | 16 651.397 | 0 | 61.5 | 16 644.732 | 0 |
| 18.5 | 16 657.601 | 1 | 100.5 | 16 656.846 | 2 | 26.5 | 16 653.278 | −3 | 69.5 | 16 646.166 | 2 | 17.5 | 16 654.551 | −4 | 18.5 | 16 651.277 | −3 | 62.5 | 16 644.547 | 2 |
| 19.5 | 16 657.656 | 0 | 101.5 | 16 656.769 | 1 | 27.5 | 16 653.150 | 1 | 70.5 | 16 645.960 | −3 | 18.5 | 16 654.617 | 4 | 19.5 | 16 651.165 | 4 | 63.5 | 16 644.356 | 1 |
| 20.5 | 16 657.711 | 1 | 102.5 | 16 656.691 | 0 | 28.5 | 16 653.013 | −3 | 71.5 | 16 645.757 | −4 | 19.5 | 16 654.666 | −3 | 20.5 | 16 651.043 | 3 | 64.5 | 16 644.165 | −1 |
| 21.5 | 16 657.765 | 1 | 103.5 | 16 656.609 | −3 | 29.5 | 16 652.878 | −3 | 72.5 | 16 645.553 | −4 | 20.5 | 16 654.728 | 3 | 21.5 | 16 650.922 | 3 | 65.5 | 16 643.971 | −2 |
| 22.5 | 16 657.816 | 2 | 104.5 | 16 656.530 | −1 | 30.5 | 16 652.741 | −3 | 73.5 | 16 645.350 | −1 | 21.5 | 16 654.774 | −3 | 22.5 | 16 650.795 | 0 | 66.5 | 16 643.783 | 3 |
| 23.5 | 16 657.866 | 2 | 105.5 | 16 656.449 | 2 | 31.5 | 16 652.603 | −3 | 74.5 | 16 645.141 | −3 | 22.5 | 16 654.830 | 0 | 23.5 | 16 650.668 | −2 | 67.5 | 16 643.586 | 2 |
| 24.5 | 16 657.915 | 3 | | | | 32.5 | 16 652.465 | −1 | 75.5 | 16 644.940 | 4 | 23.5 | 16 654.880 | 0 | 24.5 | 16 650.546 | 4 | 68.5 | 16 643.389 | 2 |
| 25.5 | 16 657.961 | 3 | $Q_{3/2}(J)$ | | | 33.5 | 16 652.321 | −4 | 76.5 | 16 644.729 | 4 | 24.5 | 16 654.925 | −3 | 25.5 | 16 650.418 | 3 | 69.5 | 16 643.192 | 3 |
| 26.5 | 16 658.005 | 2 | | | | 34.5 | 16 652.181 | −1 | 77.5 | 16 644.510 | −3 | 25.5 | 16 654.972 | −3 | 26.5 | 16 650.284 | 0 | 70.5 | 16 642.989 | 0 |
| 27.5 | 16 658.048 | 2 | 1.5 | 16 656.179 | 1 | 35.5 | 16 652.037 | 0 | 78.5 | 16 644.296 | −3 | 26.5 | 16 655.018 | −2 | 27.5 | 16 650.153 | 0 | 71.5 | 16 642.787 | −1 |
| 28.5 | 16 658.086 | −2 | | | | 36.5 | 16 651.889 | −2 | 79.5 | 16 644.085 | 0 | 27.5 | 16 655.062 | −3 | 28.5 | 16 650.016 | 4 | 72.5 | 16 642.588 | 3 |
| 29.5 | 16 658.130 | 3 | | | | 37.5 | 16 651.744 | 1 | 80.5 | 16 643.865 | −2 | 28.5 | 16 655.105 | −2 | 29.5 | 16 649.888 | 3 | 73.5 | 16 642.380 | 0 |
| 30.5 | 16 658.168 | 3 | | | | 38.5 | 16 651.592 | −2 | 81.5 | 16 643.649 | 0 | 29.5 | 16 655.146 | −1 | 30.5 | 16 649.754 | 6 | 74.5 | 16 642.175 | 1 |
| 31.5 | 16 658.205 | 3 | | | | 39.5 | 16 651.442 | −1 | 82.5 | 16 643.429 | 0 | 30.5 | 16 655.185 | −1 | 31.5 | 16 649.612 | 2 | 75.5 | 16 641.966 | 1 |
| 32.5 | 16 658.238 | 1 | | | | 40.5 | 16 651.289 | −1 | 83.5 | 16 643.207 | −1 | 31.5 | 16 655.222 | −2 | 32.5 | 16 649.472 | 1 | 76.5 | 16 641.758 | 2 |
| 33.5 | 16 658.272 | 1 | | | | 41.5 | 16 651.137 | 1 | 84.5 | 16 642.988 | 3 | 32.5 | 16 655.267 | 7 | 33.5 | 16 649.334 | 4 | 77.5 | 16 641.544 | −1 |
| 34.5 | 16 658.300 | −2 | | | | 42.5 | 16 650.982 | 2 | 85.5 | 16 642.757 | −3 | 33.5 | 16 655.293 | −1 | 34.5 | 16 649.190 | 2 | 78.5 | 16 641.334 | 2 |
| 35.5 | 16 658.332 | −1 | | | | 43.5 | 16 650.823 | 1 | 86.5 | 16 642.535 | 3 | 34.5 | 16 655.329 | 2 | 35.5 | 16 649.049 | 6 | 79.5 | 16 641.121 | 3 |
| 36.5 | 16 658.362 | 1 | | | | 44.5 | 16 650.668 | 5 | 87.5 | 16 642.307 | 1 | 35.5 | 16 655.355 | −2 | 36.5 | 16 648.899 | 2 | 80.5 | 16 640.902 | 0 |
| 37.5 | 16 658.389 | 0 | | | | 45.5 | 16 650.506 | 4 | 88.5 | 16 642.078 | 2 | 36.5 | 16 655.385 | −2 | 37.5 | 16 648.753 | 4 | | | |
| 38.5 | 16 658.415 | 2 | | | | 46.5 | 16 650.341 | 1 | 89.5 | 16 641.848 | 3 | 37.5 | 16 655.414 | −0 | 38.5 | 16 648.602 | 1 | | | |
| 39.5 | 16 658.440 | 3 | | | | 47.5 | 16 650.176 | 0 | 90.5 | 16 641.611 | −1 | 38.5 | 16 655.440 | −1 | 39.5 | 16 648.452 | 2 | | | |
| 40.5 | 16 658.462 | 3 | | | | 48.5 | 16 650.016 | 5 | 91.5 | 16 641.379 | 1 | 39.5 | 16 655.465 | −1 | 40.5 | 16 648.295 | −2 | | | |
| 41.5 | 16 658.483 | 3 | | | | 49.5 | 16 649.846 | 2 | 92.5 | 16 641.141 | −2 | 40.5 | 16 655.489 | 1 | 41.5 | 16 648.139 | −4 | | | |
| 42.5 | 16 658.502 | 3 | | | | 50.5 | 16 649.677 | 3 | 93.5 | 16 640.902 | −2 | 41.5 | 16 655.509 | −1 | 42.5 | 16 647.989 | 1 | | | |
| 81.5 | 16 657.980 | 0 | | | | 51.5 | 16 649.506 | 1 | | | | 42.5 | 16 655.530 | 0 | 43.5 | 16 647.833 | 3 | | | |
| 82.5 | 16 657.934 | −1 | | | | | | | | | | 43.5 | 16 655.545 | −3 | 44.5 | 16 647.670 | −2 | | | |

[a] $(o\text{-}c)\times 10^3$.

TABLE II. Frequencies (in $cm^{-1}$) and assignments for the $\tilde{A}\ ^2\Pi_g \leftarrow \tilde{X}\ ^2\Pi_u\ 0_0^0$ absorption spectrum of $DC_6H^+$ and residuals from the fit.

| $J$ | obs. | $o$-$c$[a] | $J$ | obs. | $o$-$c$[a] | $J$ | obs. | $o$-$c$[a] | $J$ | obs. | $o$-$c$[a] | $J$ | obs. | $o$-$c$[a] | $J$ | obs. | $o$-$c$[a] |
|---|---|---|---|---|---|---|---|---|---|---|---|---|---|---|---|---|---|
| $R_{3/2}(J)$ | | | $P_{3/2}(J)$ | | | | | | $R_{1/2}(J)$ | | | $P_{1/2}(J)$ | | | | | |
| 1.5 | 16 672.297 | −2 | 2.5 | 16 671.880 | 2 | 45.5 | 16 666.684 | 3 | 2.5 | 16 669.427 | −1 | 1.5 | 16 669.017 | 4 | 44.5 | 16 663.887 | 2 |
| 2.5 | 16 672.383 | 4 | 3.5 | 16 671.789 | 0 | 46.5 | 16 666.526 | 0 | 3.5 | 16 669.503 | −4 | 4.5 | 16 668.750 | 4 | 45.5 | 16 663.733 | 1 |
| 3.5 | 16 672.461 | 4 | 4.5 | 16 671.695 | −3 | 47.5 | 16 666.373 | 2 | 4.5 | 16 669.586 | 3 | 5.5 | 16 668.648 | −6 | 46.5 | 16 663.580 | 1 |
| 4.5 | 16 672.538 | 4 | 5.5 | 16 671.607 | 0 | 48.5 | 16 666.211 | −2 | 5.5 | 16 669.657 | −1 | 6.5 | 16 668.552 | −8 | 47.5 | 16 663.423 | 0 |
| 5.5 | 16 672.609 | 0 | 7.5 | 16 671.418 | 0 | 49.5 | 16 666.053 | −1 | 6.5 | 16 669.739 | 6 | 7.5 | 16 668.468 | 3 | 48.5 | 16 663.266 | 0 |
| 6.5 | 16 672.683 | 0 | 8.5 | 16 671.323 | 1 | 50.5 | 16 665.894 | 1 | 7.5 | 16 669.809 | 4 | 8.5 | 16 668.366 | −3 | 49.5 | 16 663.111 | 4 |
| 7.5 | 16 672.754 | 0 | 9.5 | 16 671.220 | −4 | 51.5 | 16 665.731 | −1 | 8.5 | 16 669.872 | −4 | 9.5 | 16 668.278 | 7 | 50.5 | 16 662.944 | −3 |
| 8.5 | 16 672.829 | 4 | 10.5 | 16 671.123 | −1 | 52.5 | 16 665.567 | −1 | 10.5 | 16 670.011 | −3 | 10.5 | 16 668.173 | 2 | 51.5 | 16 662.786 | 0 |
| 9.5 | 16 672.898 | 4 | 11.5 | 16 671.018 | −5 | 53.5 | 16 665.406 | 3 | 13.5 | 16 670.206 | −2 | 11.5 | 16 668.064 | −6 | 52.5 | 16 662.624 | 1 |
| 10.5 | 16 672.964 | 3 | 13.5 | 16 670.810 | −7 | 54.5 | 16 665.237 | 1 | 14.5 | 16 670.273 | 3 | 12.5 | 16 667.967 | 0 | 53.5 | 16 662.459 | 1 |
| 11.5 | 16 673.029 | 2 | 14.5 | 16 670.710 | −2 | 55.5 | 16 665.065 | −3 | 15.5 | 16 670.334 | 4 | 13.5 | 16 667.861 | −2 | 54.5 | 16 662.294 | 2 |
| 12.5 | 16 673.093 | 1 | 15.5 | 16 670.606 | 2 | 56.5 | 16 664.904 | 5 | 16.5 | 16 670.386 | −3 | 14.5 | 16 667.756 | −2 | 55.5 | 16 662.125 | 1 |
| 13.5 | 16 673.155 | 0 | 16.5 | 16 670.498 | 3 | 57.5 | 16 664.725 | −3 | 17.5 | 16 670.446 | 0 | 15.5 | 16 667.649 | −1 | 56.5 | 16 661.957 | 2 |
| 14.5 | 16 673.216 | 0 | 17.5 | 16 670.386 | 1 | 58.5 | 16 664.555 | 0 | 18.5 | 16 670.498 | −4 | 16.5 | 16 667.537 | −4 | 57.5 | 16 661.785 | 0 |
| 15.5 | 16 673.276 | 0 | 18.5 | 16 670.273 | −1 | 59.5 | 16 664.380 | −1 | 19.5 | 16 670.553 | −3 | 17.5 | 16 667.430 | −1 | 58.5 | 16 661.614 | 1 |
| 16.5 | 16 673.336 | 2 | 19.5 | 16 670.157 | −3 | 60.5 | 16 664.205 | 0 | 20.5 | 16 670.606 | −3 | 18.5 | 16 667.320 | 1 | 59.5 | 16 661.438 | −1 |
| 17.5 | 16 673.393 | 2 | 20.5 | 16 670.044 | −1 | 61.5 | 16 664.030 | 2 | 21.5 | 16 670.658 | −2 | 20.5 | 16 667.092 | 0 | 60.5 | 16 661.263 | −1 |
| 18.5 | 16 673.450 | 3 | 21.5 | 16 669.929 | 0 | 62.5 | 16 663.850 | 1 | 22.5 | 16 670.710 | 0 | 21.5 | 16 666.983 | 8 | 61.5 | 16 661.085 | −3 |
| 19.5 | 16 673.505 | 4 | 22.5 | 16 669.809 | −2 | 63.5 | 16 663.671 | 3 | 23.5 | 16 670.760 | 2 | 22.5 | 16 666.860 | 2 | 62.5 | 16 660.908 | −1 |
| 20.5 | 16 673.551 | −1 | 23.5 | 16 669.692 | 0 | 64.5 | 16 663.486 | −1 | 24.5 | 16 670.803 | −2 | 23.5 | 16 666.742 | 3 | 63.5 | 16 660.729 | 0 |
| 21.5 | 16 673.603 | 0 | 24.5 | 16 669.574 | 3 | 65.5 | 16 663.304 | 1 | 25.5 | 16 670.850 | 0 | 24.5 | 16 666.618 | 1 | 64.5 | 16 660.548 | −1 |
| 22.5 | 16 673.652 | −1 | 25.5 | 16 669.450 | 2 | 66.5 | 16 663.112 | −6 | 26.5 | 16 670.893 | 0 | 25.5 | 16 666.495 | −1 | 65.5 | 16 660.366 | 0 |
| 23.5 | 16 673.698 | −2 | 26.5 | 16 669.327 | 2 | 67.5 | 16 662.935 | 2 | 27.5 | 16 670.934 | −1 | 26.5 | 16 666.373 | 2 | 66.5 | 16 660.179 | −2 |
| 24.5 | 16 673.743 | −3 | 27.5 | 16 669.200 | 1 | 68.5 | 16 662.742 | −2 | 28.5 | 16 670.975 | −1 | 27.5 | 16 666.248 | 2 | 67.5 | 16 659.994 | −2 |
| 25.5 | 16 673.788 | −3 | 28.5 | 16 669.073 | 1 | 70.5 | 16 662.362 | −2 | 29.5 | 16 671.018 | 3 | 28.5 | 16 666.120 | 0 | 68.5 | 16 659.810 | 2 |
| 26.5 | 16 673.833 | −1 | 29.5 | 16 668.945 | 1 | 71.5 | 16 662.175 | 4 | 30.5 | 16 671.051 | −1 | 29.5 | 16 665.993 | 2 | | | |
| 27.5 | 16 673.876 | 1 | 30.5 | 16 668.813 | −1 | 72.5 | 16 661.977 | 0 | 31.5 | 16 671.090 | 1 | 30.5 | 16 665.863 | 1 | | | |
| 28.5 | 16 673.913 | −2 | 31.5 | 16 668.681 | −1 | 73.5 | 16 661.785 | 3 | 33.5 | 16 671.157 | 0 | 31.5 | 16 665.731 | 1 | | | |
| 29.5 | 16 673.955 | 1 | 32.5 | 16 668.550 | 0 | 74.5 | 16 661.583 | −2 | 34.5 | 16 671.187 | −2 | 32.5 | 16 665.596 | −1 | | | |
| 30.5 | 16 673.990 | −1 | 33.5 | 16 668.414 | 0 | 75.5 | 16 661.383 | −3 | 35.5 | 16 671.220 | 2 | 33.5 | 16 665.462 | −1 | | | |
| 31.5 | 16 674.025 | −2 | 34.5 | 16 668.278 | −1 | 76.5 | 16 661.191 | 5 | 36.5 | 16 671.250 | 3 | 34.5 | 16 665.326 | −2 | | | |
| 32.5 | 16 674.058 | −2 | 35.5 | 16 668.141 | 0 | 77.5 | 16 660.986 | 2 | 37.5 | 16 671.276 | 2 | 35.5 | 16 665.190 | −1 | | | |
| 33.5 | 16 674.093 | 1 | 36.5 | 16 668.003 | 1 | 78.5 | 16 660.779 | −2 | 38.5 | 16 671.298 | −1 | 36.5 | 16 665.049 | −1 | | | |
| 34.5 | 16 674.125 | 1 | 37.5 | 16 667.861 | 0 | 79.5 | 16 660.581 | 4 | 39.5 | 16 671.323 | 0 | 37.5 | 16 664.904 | 0 | | | |
| 35.5 | 16 674.151 | −1 | 38.5 | 16 667.719 | 0 | 80.5 | 16 660.366 | 5 | 40.5 | 16 671.348 | 3 | 38.5 | 16 664.767 | 0 | | | |
| 36.5 | 16 674.180 | −1 | 39.5 | 16 667.574 | −1 | 81.5 | 16 660.165 | 2 | 41.5 | 16 671.365 | −1 | 39.5 | 16 664.625 | −2 | | | |
| 37.5 | 16 674.208 | 2 | 40.5 | 16 667.430 | 0 | 82.5 | 16 659.952 | −2 | 42.5 | 16 671.385 | −1 | 40.5 | 16 664.480 | 0 | | | |
| 38.5 | 16 674.232 | 0 | 41.5 | 16 667.282 | −1 | | | | 43.5 | 16 671.408 | 4 | 41.5 | 16 664.332 | −3 | | | |
| 39.5 | 16 674.255 | 0 | 42.5 | 16 667.137 | 2 | $Q_{3/2}(J)$ | | | 44.5 | 16 671.418 | −2 | 42.5 | 16 664.186 | 2 | | | |
| 40.5 | 16 674.273 | −3 | 43.5 | 16 666.983 | −2 | | | | | | | 43.5 | 16 664.033 | 1 | | | |
| | | | 44.5 | 16 666.833 | 0 | 1.5 | 16 672.085 | −5 | | | | | | | | | |

[a] $(o\text{-}c)\times 10^3$.

Figs. 3(b) and 3(c) shows a significant enhancement in the case of the double modulation technique.

An examination of the gap at the position of the $Q_{3/2}$ branch head allowed the absolute numbering of the rotational lines in the sub-band to be established and hence a direct assignment of the spin-orbit component. As indicated in Fig. 3(b), the higher energy sub-band exhibits a gap of $\approx 10B$, establishing that the first transitions in the $P_{3/2}$ and $R_{3/2}$ branches are $P(2.5)$ and $R(1.5)$, respectively. In addition to the routinely assigned transitions, there remain many weak peaks in the spectrum not assigned to the $0_0^0$ band. Some of these are indicated by asterisk in Fig. 3(b). These features are dependent on the temperature in the discharge, suggesting their assignment to a hot band transition. The identification of the $Q_{1/2}$ branch heads was not possible due to the presence of such lines. Nevertheless, the low-$J$ $R_{1/2}$ and $P_{1/2}$ lines were observed and the first transitions in the $P_{1/2}$ and $R_{1/2}$ branches are $P(1.5)$ and $R(0.5)$, respectively. Based on these assignments, the sub-band at higher energy is unambiguously assigned to the $^2\Pi_{3/2} \leftarrow {}^2\Pi_{3/2}$ spin-orbit subsystem. The resulting numbering of the rotational lines is indicated partly in Fig. 2. No $\Lambda$-type splitting of the rotational lines was observed within the experimental uncertainty, even up to the high $J$ values of over 100.5.

The observed $0_0^0$ bands in the $\tilde{A}\ ^2\Pi_g \leftarrow \tilde{X}\ ^2\Pi_u$ transition of $C_6H_2^+$, $DC_6H^+$, and $C_6D_2^+$ exhibits 277, 223, and 217 assigned rovibronic transitions, respectively. The observed line positions and rotational assignments are gathered in Tables I–III. Rotational analysis of the spectra was performed by standard procedures. The line positions were fit with an effective rotational Hamiltonian where both spin-orbit systems were considered simultaneously. In the fit, the band origin ($\nu_0$), the rotational constant ($B_0$), centrifugal

TABLE III. Frequencies (in $cm^{-1}$) and assignments for the $\tilde{A}\ ^2\Pi_g \leftarrow \tilde{X}\ ^2\Pi_u\ 0_0^0$ absorption spectrum of $C_6D_2^+$ and residuals from the fit.

| $J$ | obs. | $o$-$c$[a] | $J$ | obs. | $o$-$c$[a] | $J$ | obs. | $o$-$c$[a] | $J$ | obs. | $o$-$c$[a] | $J$ | obs. | $o$-$c$[a] | $J$ | obs. | $o$-$c$[a] |
|---|---|---|---|---|---|---|---|---|---|---|---|---|---|---|---|---|---|
| $R_{3/2}(J)$ | | | $P_{3/2}(J)$ | | | | | | $R_{1/2}(J)$ | | | $P_{1/2}(J)$ | | | | | |
| 1.5 | 16 688.166 | 1 | 2.5 | 16 687.760 | −1 | 43.5 | 16 683.096 | 3 | 0.5 | 16 685.179 | 5 | 1.5 | 16 684.928 | −3 | 39.5 | 16 680.741 | −2 |
| 2.5 | 16 688.240 | 0 | 3.5 | 16 687.678 | 1 | 44.5 | 16 682.949 | 1 | 1.5 | 16 685.253 | −1 | 2.5 | 16 684.847 | −1 | 40.5 | 16 680.605 | −1 |
| 3.5 | 16 688.311 | −4 | 4.5 | 16 687.590 | 0 | 45.5 | 16 682.802 | 0 | 2.5 | 16 685.322 | −6 | 3.5 | 16 684.763 | 0 | 41.5 | 16 680.466 | 0 |
| 4.5 | 16 688.390 | 2 | 5.5 | 16 687.502 | 0 | 46.5 | 16 682.652 | −3 | 3.5 | 16 685.398 | −5 | 4.5 | 16 684.671 | −5 | 42.5 | 16 680.323 | −2 |
| 5.5 | 16 688.463 | 3 | 6.5 | 16 687.415 | 2 | 47.5 | 16 682.505 | −2 | 4.5 | 16 685.478 | 1 | 5.5 | 16 684.584 | −4 | 43.5 | 16 680.181 | −1 |
| 6.5 | 16 688.533 | 2 | 9.5 | 16 687.133 | −3 | 48.5 | 16 682.357 | 0 | 5.5 | 16 685.555 | 6 | 6.5 | 16 684.498 | −1 | 44.5 | 16 680.038 | −1 |
| 7.5 | 16 688.600 | 0 | 10.5 | 16 687.045 | 3 | 49.5 | 16 682.205 | 0 | 6.5 | 16 685.620 | 1 | 7.5 | 16 684.404 | −4 | 45.5 | 16 679.894 | 1 |
| 8.5 | 16 688.666 | −1 | 11.5 | 16 686.949 | 4 | 50.5 | 16 682.052 | −1 | 7.5 | 16 685.684 | −5 | 8.5 | 16 684.317 | 2 | 46.5 | 16 679.747 | 1 |
| 9.5 | 16 688.735 | 1 | 12.5 | 16 686.848 | 1 | 51.5 | 16 681.900 | 2 | 8.5 | 16 685.757 | 0 | 9.5 | 16 684.227 | 5 | 47.5 | 16 679.596 | −2 |
| 10.5 | 16 688.800 | 2 | 13.5 | 16 686.746 | −2 | 52.5 | 16 681.743 | 1 | 9.5 | 16 685.822 | −1 | 10.5 | 16 684.131 | 4 | 48.5 | 16 679.449 | 0 |
| 11.5 | 16 688.863 | 2 | 14.5 | 16 686.646 | −1 | 53.5 | 16 681.586 | 2 | 10.5 | 16 685.886 | 2 | 11.5 | 16 684.027 | −3 | 49.5 | 16 679.297 | 0 |
| 12.5 | 16 688.923 | 0 | 15.5 | 16 686.546 | 1 | 54.5 | 16 681.421 | −5 | 11.5 | 16 685.952 | 0 | 12.5 | 16 683.931 | −1 | 50.5 | 16 679.145 | 1 |
| 13.5 | 16 688.983 | 0 | 16.5 | 16 686.441 | 0 | 55.5 | 16 681.271 | 5 | 12.5 | 16 686.012 | −2 | 13.5 | 16 683.831 | −2 | 51.5 | 16 678.992 | 1 |
| 14.5 | 16 689.041 | −1 | 17.5 | 16 686.334 | −2 | 56.5 | 16 681.108 | 3 | 13.5 | 16 686.075 | 1 | 14.5 | 16 683.733 | 1 | 52.5 | 16 678.837 | 1 |
| 15.5 | 16 689.098 | −2 | 18.5 | 16 686.227 | −2 | 57.5 | 16 680.944 | 3 | 14.5 | 16 686.130 | −4 | 15.5 | 16 683.628 | −2 | 53.5 | 16 678.680 | 1 |
| 16.5 | 16 689.157 | 1 | 19.5 | 16 686.121 | 1 | 58.5 | 16 680.775 | −2 | 15.5 | 16 686.194 | 2 | 16.5 | 16 683.519 | −6 | 54.5 | 16 678.518 | −2 |
| 17.5 | 16 689.212 | 2 | 20.5 | 16 686.012 | 1 | 59.5 | 16 680.608 | −3 | 16.5 | 16 686.252 | 4 | 17.5 | 16 683.423 | 2 | 55.5 | 16 678.361 | 1 |
| 18.5 | 16 689.265 | 2 | 21.5 | 16 685.899 | −2 | 60.5 | 16 680.442 | −1 | 17.5 | 16 686.302 | −1 | 18.5 | 16 683.316 | 2 | 56.5 | 16 678.200 | 0 |
| 19.5 | 16 689.315 | 0 | 22.5 | 16 685.790 | 3 | 61.5 | 16 680.273 | −2 | 18.5 | 16 686.356 | −1 | 19.5 | 16 683.207 | 2 | 57.5 | 16 678.036 | −1 |
| 20.5 | 16 689.365 | 0 | 23.5 | 16 685.673 | −1 | 62.5 | 16 680.104 | 0 | 19.5 | 16 686.409 | 0 | 20.5 | 16 683.096 | −1 | 58.5 | 16 677.873 | −1 |
| 21.5 | 16 689.415 | 1 | 24.5 | 16 685.557 | −2 | 63.5 | 16 679.933 | 0 | 20.5 | 16 686.460 | 1 | 21.5 | 16 682.989 | 4 | 59.5 | 16 677.704 | −4 |
| 22.5 | 16 689.462 | 1 | 25.5 | 16 685.438 | −4 | 64.5 | 16 679.756 | −4 | 21.5 | 16 686.509 | 0 | 22.5 | 16 682.874 | 1 | 60.5 | 16 677.539 | −2 |
| 23.5 | 16 689.507 | 0 | 26.5 | 16 685.322 | −2 | 65.5 | 16 679.584 | −1 | 22.5 | 16 686.552 | −4 | 23.5 | 16 682.760 | 1 | 61.5 | 16 677.372 | 0 |
| 24.5 | 16 689.552 | 1 | 27.5 | 16 685.201 | −3 | 66.5 | 16 679.409 | 0 | 23.5 | 16 686.602 | 0 | 24.5 | 16 682.651 | 7 | 62.5 | 16 677.199 | −4 |
| 25.5 | 16 689.594 | −1 | 28.5 | 16 685.080 | −3 | 67.5 | 16 679.232 | 1 | 24.5 | 16 686.646 | −2 | 25.5 | 16 682.530 | 3 | 63.5 | 16 677.032 | 0 |
| 26.5 | 16 689.635 | 0 | 29.5 | 16 684.958 | −2 | 68.5 | 16 679.052 | 0 | 25.5 | 16 686.690 | −1 | 26.5 | 16 682.409 | −1 | 64.5 | 16 676.859 | −1 |
| 27.5 | 16 689.675 | 0 | 30.5 | 16 684.835 | −2 | 69.5 | 16 678.873 | 2 | 26.5 | 16 686.736 | 3 | 27.5 | 16 682.288 | −1 | 65.5 | 16 676.690 | 4 |
| 28.5 | 16 689.715 | 1 | 31.5 | 16 684.709 | 1 | 70.5 | 16 678.691 | 1 | 27.5 | 16 686.778 | 4 | 28.5 | 16 682.167 | −2 | 66.5 | 16 676.513 | 3 |
| 29.5 | 16 689.752 | 1 | 32.5 | 16 684.584 | 1 | 71.5 | 16 678.506 | −1 | 28.5 | 16 686.811 | −2 | 29.5 | 16 682.052 | 5 | 67.5 | 16 676.333 | 0 |
| 30.5 | 16 689.787 | 0 | 33.5 | 16 684.453 | −3 | 72.5 | 16 678.323 | 1 | 29.5 | 16 686.848 | −3 | 30.5 | 16 681.925 | 2 | 68.5 | 16 676.155 | 0 |
| 31.5 | 16 689.822 | 1 | 34.5 | 16 684.324 | −2 | 73.5 | 16 678.134 | −2 | 30.5 | 16 686.889 | 2 | 31.5 | 16 681.800 | 3 | 69.5 | 16 675.979 | 4 |
| 32.5 | 16 689.857 | 3 | 35.5 | 16 684.194 | 0 | 74.5 | 16 677.948 | −1 | 31.5 | 16 686.924 | 2 | 32.5 | 16 681.674 | 3 | 70.5 | 16 675.794 | 0 |
| 33.5 | 16 689.884 | −2 | 36.5 | 16 684.061 | −1 | 75.5 | 16 677.756 | −3 | 32.5 | 16 686.953 | −2 | 33.5 | 16 681.544 | 1 | | | |
| 34.5 | 16 689.915 | 0 | 37.5 | 16 683.929 | 1 | 76.5 | 16 677.573 | 4 | 33.5 | 16 686.986 | −1 | 34.5 | 16 681.416 | 4 | | | |
| 35.5 | 16 689.945 | 2 | 38.5 | 16 683.791 | −1 | | | | 34.5 | 16 687.018 | 0 | 35.5 | 16 681.280 | −2 | | | |
| | | | 39.5 | 16 683.654 | −1 | | | | 35.5 | 16 687.046 | −1 | 36.5 | 16 681.153 | −3 | | | |
| $Q_{3/2}(J)$ | | | 40.5 | 16 683.519 | 3 | | | | 36.5 | 16 687.073 | −2 | 37.5 | 16 681.018 | 2 | | | |
| | | | 41.5 | 16 683.378 | 1 | | | | 37.5 | 16 687.099 | −2 | 38.5 | 16 680.878 | −2 | | | |
| 1.5 | 16 687.962 | −2 | 42.5 | 16 683.237 | 2 | | | | | | | | | | | | |

[a] $(o\text{-}c)\times 10^3$.

distortion constant ($D_0$), and spin-orbit interaction constant ($A_0$) of both states were adjustable parameters. The Λ-type doubling terms were neglected, because splittings were not detected in the spectra. The line positions of all observed lines could be fit to standard deviations that are significantly less than the observed linewidths. The differences between the observed and calculated line positions for $C_6H_2^+$, $DC_6H^+$, and $C_6D_2^+$ are also given in Tables I–III. The standard deviation of the fits are 0.0024, 0.0025, and 0.0023 $cm^{-1}$, respectively. Figure 4(a) displays a selected portion of the $0_0^0$ band of $C_6H_2^+$ in a region of overlapping rotational structure of the two spin-orbit sub-bands. The real absorption spectrum derived from the FM data is shown in Fig. 4(b). Also shown in Fig. 4(c) is the corresponding calculated spectrum, based on the fit of the band and the determined line shape. The rotational temperature of $C_6H_2^+$ in the discharge was estimated from the relative intensities of the absorption lines to be 170±20 K. The computed spectrum is in reasonable agreement with the experiment.

The derived values of the best fit molecular constants are listed in Table IV. The spin-orbit interaction constant, $A_0''$, of $C_6H_2^+$ is $-31.4\ cm^{-1}$ for the $\tilde{X}\ ^2\Pi_u$ state. Substitution of the hydrogens by one or two deuterium atoms has little effect on the magnitude of $A_0$, within the experimental uncertainty. The magnitude of $A_0''$ is similar to that of diacetylene cation in its $\tilde{X}\ ^2\Pi_g$ state; $-33.3(8)\ cm^{-1}$.[2,4] Excitation to the $\tilde{A}\ ^2\Pi_g$ state of $C_6H_2^+$ results in a large change in the magnitude of $A_0'(-3.0\ cm^{-1})$. A similar trend is also observed for $C_4H_2^+$ in its $\tilde{A}\ ^2\Pi_u$ state, $A_0'(-2.7\ cm^{-1})$. These values are close to the spin-orbit interaction constant of the carbon atom ($29\ cm^{-1}$), evidencing that $C_6H_2^+$ is essentially the $\pi$ electron radical in both electronic states.

The derived rotational constant of $C_6H_2^+$ in the $\tilde{X}\ ^2\Pi_u$ state is $B_0''=0.044\ 59\ cm^{-1}$ and decreases in the $\tilde{A}\ ^2\Pi_g$ state to $0.043\ 79\ cm^{-1}$. Substitution of one or two deuterium atoms has a substantial effect on the rotational constant. The observed rotational constant reflects the changes in the C≡C

TABLE IV. Molecular constants (in $cm^{-1}$) of $C_6H_2^+$, $HC_6D^+$, and $C_6D_2^+$ in the $\tilde{X}\ ^2\Pi_u$ and $\tilde{A}\ ^2\Pi_g$ states, derived from analysis of the rotationally resolved $\tilde{A}\ ^2\Pi_g \leftarrow \tilde{X}\ ^2\Pi_u$ FM absorption spectra. $N$ is the number of lines used in the fit; $o-c$ is the observed minus calculated standard deviation of the fit (in $cm^{-1}$).[a]

| | $C_6H_2^+$ | $DC_6H^+$ | $C_6D_2^+$ |
|---|---|---|---|
| | | $\tilde{X}\ ^2\Pi_u$ state | |
| $B_0''$ | 0.044 594 3(34) | 0.042 573 9(79) | 0.040 701 4(87) |
| $D_0'' \times 10^9$ | 2.56(27) | 2.90(26) | 2.60(63) |
| $A_0''$ | −31.40(28) | −32.37(56) | −31.31(49) |
| | | $\tilde{A}\ ^2\Pi_g$ state | |
| $B_0'$ | 0.043 792 1(34) | 0.041 814 7(81) | 0.039 980 6(88) |
| $D_0' \times 10^9$ | 2.43(26) | 3.00(27) | 2.80(67) |
| $A_0'$ | −28.41(28) | −29.42(56) | −28.40(49) |
| $\nu_0$ | 16 654.687 26(25) | 16 670.616 76(30) | 16 686.510 04(28) |
| $N$ | 277 | 223 | 217 |
| $o-c$ | 0.0024 | 0.0025 | 0.0023 |

[a]One standard deviation given in parentheses.

and C–C bond lengths of the ion relative to the neutral species. Neutral triacetylene has the molecular orbital configuration $\ldots(\pi_u)^4(\pi_g)^4(\pi_u)^4$, where the highest orbital is bonding in the C≡C but antibonding in the C–C regions.[21] The C≡C bond lengths increase in the $\tilde{X}\ ^2\Pi_u$ and $\tilde{A}\ ^2\Pi_g$ states of $C_6H_2^+$ with respect to the neutral value. In contrast, the C–C bond decreases in the $\tilde{X}\ ^2\Pi_u$ state but increases in the $\tilde{A}\ ^2\Pi_g$ state relative to the neutral values. The C–H bond lengths remain relatively unchanged. The changes in bond lengths are reflected in the vibrational frequency changes of the $\nu$(C≡C) and $\nu$(C–C) modes of $C_6H_2^+$ relative to the neutral values.[6]

The present results are qualitatively consistent with these views. The rotational constant of $C_6H_2^+$ in the $\tilde{X}\ ^2\Pi_u$ state is comparable to the rotational constant of the corresponding neutral species, $B_0''(C_6H_2) = 0.044\ 172\ 23(15)\,cm^{-1}$.[22] This observation is in agreement with the changes in the C≡C and C–C bond lengths, upon ionization. The relative changes compensate each other, resulting in little change in the overall length of the molecule. Excitation to the $\tilde{A}\ ^2\Pi_g$ state produces a small decrease ($0.0008\ cm^{-1}$) in $B_0$. This observation reflects the increases in both the C≡C and C–C bond lengths, resulting in a measurable increase in the overall length of the molecule upon $\tilde{A}\ ^2\Pi_g \leftarrow \tilde{X}\ ^2\Pi_u$ excitation.

The overall length of $C_6H_2^+$ in the $\tilde{A}\ ^2\Pi_g$ and $\tilde{X}\ ^2\Pi_u$ states is determined by deriving the center-of-mass (COM) coordinates of the two hydrogen atoms using Kraitchman's equations.[23] Comparison of the observed rotational constants of $C_6H_2^+$, $DC_6H^+$, and $C_6D_2^+$ allows two such determinations, one from the $C_6H_2^+/DC_6H^+$ pair and one from $C_6H_2^+/C_6D_2^+$. The coordinates are calculated from the deduced expressions for linear symmetric molecules,

$$z^2 = [1/(m^* - m)][1/B_0^* - 1/B_0], \tag{1}$$

$$z^2 = \{m^*/[m(m^* - m)]\}\{1/B_0^* - 1/B_0\}, \tag{2}$$

where $z$ is the position of the unsubstituted atom in the COM frame and $m$ and $m^*$ are the masses, and $B_0$ and $B_0^*$ are the moments of inertia of the unsubstituted and substituted derivatives, respectively. Equations (1) and (2) are applicable for the $C_6H_2^+/C_6D_2^+$ and $C_6H_2^+/DC_6H^+$ pairs, respectively, and yield a value of $|z|$ in the $\tilde{X}\ ^2\Pi_u$ ($\tilde{A}\ ^2\Pi_g$) state of 424(427) and 425(428) pm. The independent determinations yield the same result, within experimental error of 1 pm. The average H–H distance for $C_6H_2^+$ in the $\tilde{X}\ ^2\Pi_g$ state is 849(2) pm and increases in the $\tilde{A}\ ^2\Pi_u$ state to 855(2) pm.

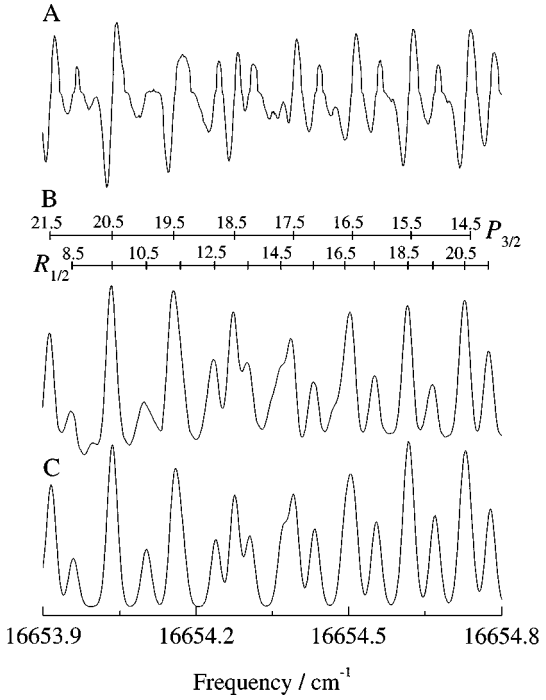


FIG. 4. Selected portion of the $\tilde{A}\ ^2\Pi_g \leftarrow \tilde{X}\ ^2\Pi_u$ $0_0^0$ band of $C_6H_2^+$ in the region of overlapping rotational structure of the $P_{3/2}$ and $R_{1/2}$ pair of branches. (a) FM absorption signal. (b) Integration of the FM spectrum in (a). Rotational assignments are indicated above each branch. (c) Corresponding calculated spectrum.

## IV. SUMMARY

The rotationally resolved $\tilde{A}\ ^2\Pi_g \leftarrow \tilde{A}\ ^2\Pi_u\ 0_0^0$ electronic absorption spectrum of $C_6H_2^+$ and its isotopic derivatives $DC_6H^+$ and $C_6D_2^+$ has been obtained. A double modulation scheme based on production modulation in a discharge cell and frequency modulation of a continuous wave ring-dye laser has been employed. The combined technique has been shown to improve the signal-to-noise ratio significantly over the conventional technique used for the spectroscopy of transients. Analyses of the spectra provide accurate information on the molecular constants and geometries of the triacetylene cation.

## ACKNOWLEDGMENTS

The authors thank Dr. G. E. Hall for much technical advice and Dr. T. Sears for bringing the frequency modulation technique to our attention; both are at Brookhaven National Laboratory. This work was supported by the Swiss National Science Foundation, Project No. 20-49104.96.

[1] H. Schüler and L. Reinbeck, Z. Naturforsch. **6**a, 160 (1951); **7**a, 285 (1952); **9**a, 350 (1954).
[2] J. H. Callomon, Can. J. Phys. **34**, 1046 (1956).
[3] M. Allan, E. Kloster-Jensen, and J. P. Maier, J. Chem. Phys. **11**, 7 (1976).
[4] R. Kuhn, J. P. Maier, and M. Ochsner, Mol. Phys. **59**, 441 (1986).
[5] J. Lecoultre, J. P. Maier, and M. Rösslein, J. Chem. Phys. **89**, 6081 (1988).
[6] D. Klapstein, R. Kuhn, J. P. Maier, M. Ochsner, and W. Zambach, J. Phys. Chem. **88**, 5176 (1984).
[7] G. C. Bjorklund, Opt. Lett. **5**, 15 (1980); G. C. Bjorklund and M. D. Levenson, Phys. Rev. A **24**, 166 (1981).
[8] J. L. Hall, L. Hollberg, T. Baer, and H. G. Robinson, Appl. Phys. Lett. **39**, 680 (1981).
[9] M. C. McCarthy, J. C. Bloch, and R. W. Field, J. Chem. Phys. **100**, 6331 (1994).
[10] M. C. McCarthy and R. W. Field, J. Chem. Phys. **100**, 6347 (1994).
[11] J. C. Bloch, R. W. Field, G. E. Hall, and T. J. Sears, J. Chem. Phys. **101**, 1717 (1994).
[12] E. A. Whittaker, H. R. Wendt, H. E. Hunziker, and G. C. Borklund, Appl. Phys. B: Photophys. Laser Chem. **35**, 105 (1984).
[13] E. A. Whittaker, B. J. Sullivan, G. C. Borklund, H. R. Wendt, and H. E. Hunziker, J. Chem. Phys. **80**, 961 (1984).
[14] J. M. Jasinski, E. A. Whittaker, G. C. Borklund, R. W. Dreyfus, R. D. Estes, and R. E. Walkup, Appl. Phys. Lett. **44**, 1155 (1984).
[15] B.-C. Chang, M. Wu, G. E. Hall, and T. J. Sears, J. Chem. Phys. **101**, 9236 (1994).
[16] B.-C. Chang and T. J. Sears, J. Chem. Phys. **102**, 6347 (1995).
[17] B.-C. Chang and T. J. Sears, J. Mol. Spectrosc. **173**, 391 (1995).
[18] B.-C. Chang and T. J. Sears, Chem. Phys. Lett. **256**, 288 (1996).
[19] S. W. North, X. S. Zheng, R. Fei, and G. E. Hall, J. Chem. Phys. **104**, 2129 (1996).
[20] C. M. Western, School of Chemistry, University of Bristol, England, PGOPHER v3,73 (1994).
[21] F. Brogli, E. Heilbronner, V. Hornung, and E. Kloster-Jensen, Helv. Chim Acta **56**, 2171 (1973).
[22] D. McNaughton and D. N. Bruget, J. Mol. Spectrosc. **150**, 620 (1991).
[23] J. Kraitchman, Am. J. Phys. **21**, 17 (1953).